Enhancing the chroma of pigmented polymers using antireflective surface structures

Clausen, Jeppe Sandvik; Christiansen, Alexander Bruun; Kristensen, Anders; Mortensen, N. Asger

Published in:
Applied Optics

Link to article, DOI:
10.1364/AO.52.007832

Publication date:
2013

Document Version
Publisher's PDF, also known as Version of record

Enhancing the chroma of pigmented polymers using antireflective surface structures

Jeppe S. Clausen,[1,*] Alexander B. Christiansen,[2] Anders Kristensen,[2] and N. Asger Mortensen[1]

[1]Department of Photonics Engineering, Technical University of Denmark, Oersteds Plads, Building 343, DK-2800 Kgs. Lyngby, Denmark

[2]Department of Micro and Nanotechnology, Technical University of Denmark, Oersteds Plads, Building 345B, DK-2800 Kgs. Lyngby, Denmark

*Corresponding author: jepcl@fotonik.dtu.dk

Received 13 August 2013; revised 9 October 2013; accepted 15 October 2013; posted 16 October 2013 (Doc. ID 195160); published 8 November 2013

In this paper we investigate how the color of a pigmented polymer is affected by reduction of the reflectance at the air–polymer interface. Both theoretical and experimental investigations show modified diffuse-direct reflectance spectra when the reflectance of the surface is lowered. Specifically it is found that the color change is manifested as an increase in chroma, leading to a clearer color experience. The experimental implementation is done using random tapered surface structures replicated in polymer from silicon masters using hot embossing. © 2013 Optical Society of America

OCIS codes: (330.1690) Color; (120.5700) Reflection; (310.1210) Antireflection coatings; (310.6628) Subwavelength structures, nanostructures.

http://dx.doi.org/10.1364/AO.52.007832

1. Introduction

Colored plastic is present everywhere in modern society. Many consumer products are fabricated using pigmented polymers and the appearance is an important parameter in the customer valuation of the product. In this work we suggest a method for increasing the chroma of pigmented polymers by the use of antireflective structures (ARS) in the surface of the polymer. The method may be used as selective decoration of certain areas of a surface or across the entire surface of the polymer part for general modification of the appearance.

Subwavelength ARS inspired by the eye of the moth [1] have previously been investigated in great detail as a cost-efficient alternative to expensive single or multilayer coatings deposited using vacuum equipment. The structures can, when employed on optical components such as lenses, greatly reduce the surface reflections [2–4]. Also within silicon [5–7] and III-V [8,9] technologies ARS are used, e.g., for increasing the efficiency of photovoltaic devices.

Antireflective coatings are used in various consumer products to improve functionality or appearance. In display technology antireflective coatings fabricated using thin film technologies can be used to improve the contrast ratio [10,11]. Within the textile industry various coatings applied to fabrics made from dyed polyethylene terephthalate have been used to improve the color by limiting surface reflections from the single fabric fibers [12].

In this work the ARS are introduced in the surface of colored plastic in order to modify the way the incoming light is transmitted into the polymer, thereby also modifying the interaction with the pigment. When light is incident onto a surface of a pigmented dielectric material a certain amount, determined by the refractive index and incident

1559-128X/13/327832-06$15.00/0

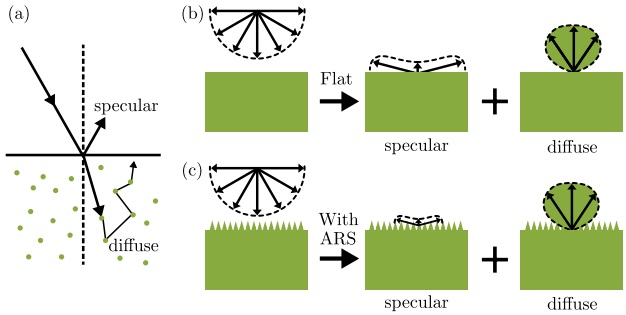

Fig. 1. (a) Illustration of specular and diffuse reflection of a light ray for a pigmented polymer. (b) Surface and bulk reflections of a pigmented polymer under diffuse illumination in the case of flat surface. (c) The surface reflectance is lowered in the presence of ARS.

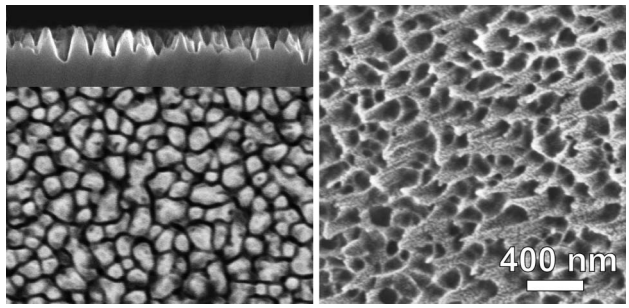

Fig. 2. Left: scanning electron micrographs of a silicon master seen from the top and from the side. Right: ABS surface after embossing (a thin layer of gold has been applied for imaging). The scale bar applies to all images. The random subwavelength nature of the ARS is evident.

angle, is reflected due to Fresnel reflection, as illustrated in Fig. 1(a). The light transmitted through the surface interacts with the pigment in a scattering process and a diffuse flux is reflected with the color of the pigment. In daily life, the incoming illumination may often be approximated by perfect diffuse illumination, as in Fig. 1(b). An observer will see the sum of the specular and the diffuse bulk reflections due to this incident radiance. By reducing the reflection at the surface, the amount of light that does not interact with the pigment is reduced and the color appearance will change, see Fig. 1(c).

The surface structures used in this study have low aspect ratio and the fabrication may therefore be done by high-throughput replication methods, such as embossing or injection molding. The effect is demonstrated in acrylonitrile butadiene styrene (ABS), one of the most widely used thermoplastics for consumer products.

2. Experimental Procedure

The ARS were fabricated on silicon wafers and then replicated in ABS in a hot embossing replication step [13]. The structures were fabricated using reactive ion etching, in a gas mixture of O_2 and SF_6 leading to randomized tapered subwavelength structures. The antireflective properties of this type of structure replicated in transparent materials have been investigated in earlier work where it was found that the reflection was reduced by a factor of 2 and only a small amount of scattering was introduced [14]. This type of structure was chosen due to the random subwavelength nature, thereby avoiding the existence of distinct diffraction orders, which would be present in holographically generated periodic structures. The surface structures are seen in scanning electron micrographs of a nanostructured silicon master in the left part of Fig. 2. The tapered structures are approximately 200 nm high. After etching, the silicon wafers were coated with perfluorodecyltrichlorosilane (FDTS) using molecular vapor deposition for easy release of the stamp after embossing.

Blue, green, and red flat substrates (5 cm diameter) for embossing were fabricated by injection molding. They were fabricated using the same unpigmented ABS and colored using master batches of the three different colors.

Hot embossing was performed in a parallel plate press at a temperature of 120°C and a constant force of 2.5 kN (corresponding to a pressure of approximately 13 bar) for 10 min followed by cooling to 80°C before releasing the pressure. A top view of the embossed surface is seen in the right part of Fig. 2. Samples with flat surfaces were fabricated using the same parameters, but with polished FDTS coated silicon wafers as stamps.

The diffuse-direct reflectance of the samples was measured using an integrating sphere (ISP-50-8-R-GT, Ocean Optics) with diffuse illumination of the sample and the detecting fiber at 8 deg with respect to the surface normal. The specular component was included in the measurements. This configuration, typically denoted $d{:}8$ [15], simulates daylight conditions in a situation with no direct light sources and near to normal observation. This configuration is chosen to include the specular contribution to the observed reflection in the color evaluation since this is a major contribution to the color changes described here. The light source was an unfiltered xenon lamp (HPX-2000, Ocean Optics), and for detection we used a spectrometer (Jaz, Ocean Optics). A white reflectance standard (WS-1, Ocean Optics) was used as reference sample.

The surface gloss was measured as the difference in reflectance with and without the specular component included in a direct-diffuse ($8{:}d$) measurement using the same integrating sphere. For the flat surface it was just below 4% corresponding to the Fresnel reflectance of the surface. For the structured surface it was below 0.5%. This reduction in gloss is mainly due to reduction in the surface reflectance, not scattering at the surface.

3. Theoretical Treatment

The goal is to determine how a modification of the surface reflectance will change the observed color under given lighting conditions. The system under consideration is a slab of pigmented polymer surrounded by air. The polymer has refractive index n.

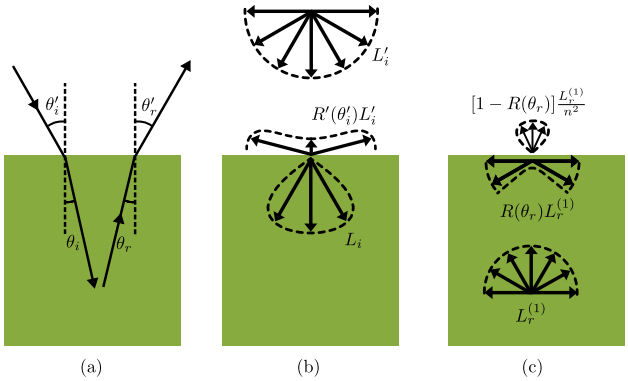

Fig. 3. (a) Definition of the angles of the incident and reflected light. (b) Illustration of the transmission of diffusive flux through the surface of the polymer. (c) The first-order diffuse reflectance from the bulk and the transmission and reflection of this flux. Figure inspired by [15].

The altered reflection properties of the surface after introduction of ARS are modeled by introduction of a parameter α, which is simply the ratio between the new reflectance and the normal Fresnel reflectance. For external reflections of the light incident at angle θ_i' [see Fig. 3(a)] the lowered reflectance R' becomes

$$R'(\theta_i') = \alpha R_f'(\theta_i'), \tag{1}$$

where R_f' is the external Fresnel reflectance for unpolarized light at the corresponding flat interface. For the internal case with the reflected light approaching the surface at an angle θ_r, the new reflectance R becomes

$$R(\theta_r) = \begin{cases} \alpha R_f(\theta_r) & \text{for } \theta_r \le \theta_c \\ 1 & \text{for } \theta_r > \theta_c \end{cases}, \tag{2}$$

where $\theta_c = \arcsin(1/n)$ is the critical angle and R_f is the internal Fresnel reflectance of unpolarized light. Here it is assumed that no scattering is introduced by the structures, thereby maintaining total internal reflection. This causes an apparent discontinuity at the critical angle for $\alpha < 1$. In reality there is a small amount of scattering, which will enable outcoupling of light near the critical angle thereby smearing out this discontinuity. The no scattering assumption is based on a small dominating period of the random structures of 180 nm, obtained from the power spectral density [14] opposed to surfaces with random structures on longer length scales [16].

The no scattering assumption also implies that Snell's law is still valid and can be applied for all light transmitted through the surface. It is also assumed that α is independent on the incident angle.

The illumination that will be used throughout the rest of this paper is diffuse light, as illustrated in Fig. 3(b). The incident diffuse light has a constant radiance, L_i', which will give rise to a partly diffuse flux below the surface with angle-dependent radiance L_i given by

$$L_i(\theta_i) = \begin{cases} [1 - R'(\theta_i')]n^2 L_i' & \theta_i \le \theta_c \\ 0 & \theta_i > \theta_c \end{cases}. \tag{3}$$

The scattering of light in the pigmented material is described using the scattering theory developed by Chandrasekhar [17], assuming isotropic scattering. In the case of a semi-infinite substrate the diffusely reflected light can be described by one parameter, the wavelength dependent single scattering albedo, ρ, defined as

$$\rho = \frac{S}{S+K}, \tag{4}$$

where S and K are the scattering and absorption coefficients, respectively. For the conservative case we therefore have $\rho = 1$, while pure absorption is characterized by $\rho = 0$. In the case of a slab of finite thickness one will, in addition to the single scattering albedo, need the optical thickness of the slab to characterize the system. However, in this description we will approximate all samples as semi-infinite substrates. Inside the scattering medium the bidirectional reflectance distribution function, f_r, [18] is given by [17]

$$f_r = \frac{dL_r}{dE_i} = \frac{\rho}{4\pi}\frac{1}{\mu_i + \mu_r} H_\rho(\mu_i) H_\rho(\mu_r). \tag{5}$$

Here, dL_r is the reflected radiance due to incident irradiance dE_i and $\mu = \cos(\theta)$. The function $H_\rho(\mu)$ is dependent on ρ and the level of approximation applied to the radiative transfer equation. While the scattering particles in the description of Chandrasekhar are embedded in a medium with refractive index being the same inside and outside of the scattering atmosphere, Wolff [19] derived a closed-form expression for the case of different refractive indices, thereby including the Fresnel reflection at the boundary between the incident and scattering media. The reflected light from the bulk is partly internally reflected at the surface and higher-order diffuse reflections are present. By summing all these higher-order contributions the reflected radiance can be found, and for $\rho > 0.6$ the closed-form expression derived by Wolff is a good approximation. The same approach is taken here except that all integrals are evaluated numerically in order to include low single scattering albedo. The first-order diffusive reflected radiance below the surface is given by

$$\begin{aligned} dL_r^{(1)} &= f_r(\cos\theta_i, \cos\theta_r) dE_i \\ &= f_r(\cos\theta_i, \cos\theta_r) L_i \cos\theta_i d\omega_i, \end{aligned} \tag{6}$$

and by integration over all solid angles the reflected part is found to be

$$L_r^{(1)} = 2\pi \int_0^{\frac{\pi}{2}} f_r(\cos\,\theta_i, \cos\,\theta_r) L_i \cos\,\theta_i\, \sin\,\theta_i \mathrm{d}\theta_i. \quad (7)$$

Following the method of Wolff [19] a part of this reflected diffuse flux escapes the medium through the surface and a part is reflected to interact with the scattering medium once again, and so on. This is illustrated in Fig. 3(c). The radiance of the j'th order reflection is found as in Eq. (7), except that the incoming radiance is now the part of $(j-1)$'th order reflected back into the bulk at the surface, leading to

$$L_r^{(j)} = 2\pi \int_0^{\frac{\pi}{2}} f_r(\cos\,\theta_i, \cos\,\theta_r) \times R(\theta_i) L_r^{(j-1)} \cos\,\theta_i\, \sin\,\theta_i \mathrm{d}\theta_i. \quad (8)$$

Note that θ_i of the j'th order equals θ_r of the $(j-1)$'th order. By summing up all contributions that escape the medium, the expression for the reflected radiance that will reach the observer becomes

$$L_r' = R'(\theta_r') L_i' + \sum_{j=1}^{\infty} [1 - R(\theta_r)] \frac{L_r^{(j)}}{n^2}, \quad (9)$$

where the first term represents the specular reflection at the surface and the second term is the sum of the diffuse contributions from the bulk.

4. Results

In order to extract the wavelength-dependent ρ for each of the colorants, the reflectance of the colored samples with planar surfaces was measured at 8 deg for diffuse incoming light. The single scattering albedo was determined for each wavelength by use of the theoretical model setting $\alpha = 1$. With the values of the single scattering albedos it is possible, by use of Eq. (9), to determine the change in reflected spectra with different values for the reduction in surface reflection. In Fig. 4 are the spectra of each of the colored flat samples shown along with two calculated spectra, of which the reflectance is reduced by a factor 2 ($\alpha = 0.5$) and completely removed ($\alpha = 0$). It is seen that the effect of this reduction in surface reflectance is a lowering of the reflectance for wavelengths that have low reflectance in the first place. For example, the reflectance of wavelengths shorter than 570 nm for the red sample is lowered significantly and the intensity ratio between short and long wavelengths is shifted. For the short wavelengths, basically all reflected light is due to the surface reflection as it is absorbed by the pigment. Therefore, the amount of reflected light of these wavelengths drops significantly, when lowering α. In general, for chromatic colors it is the significant spectral variations that lead to the color. An increase in the ratio between the high and low reflectance regions of a spectrum will make the spectral variations even more significant and therefore make the color appear more pure or clear corresponding to an increase in chroma.

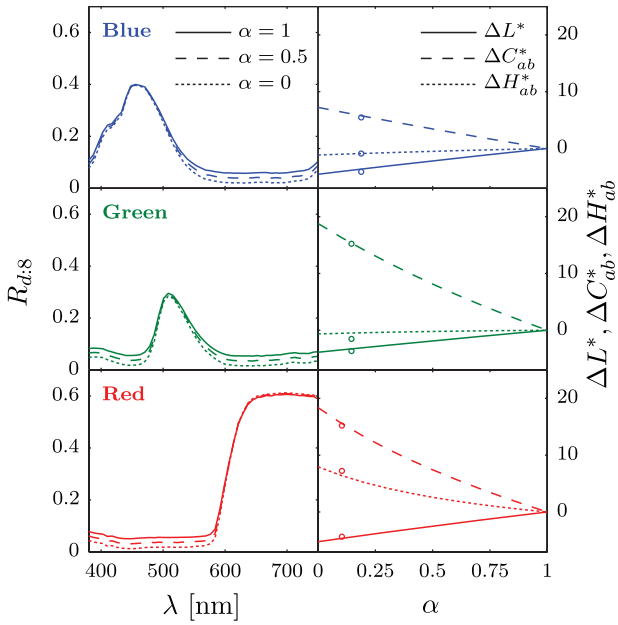

Fig. 4. Based on measured reflectance spectra are the changes in these spectra due to modifications in the surface reflectance calculated based on the proposed theoretical model. The components of the color changes for the three colors due to the lowering of α are shown. The circles mark the experimentally measured color changes plotted at the α with the best fit.

The color difference between the samples with and without ARS is evaluated based on the CIELAB 1976 color space using the cylindrical coordinates, L^*, C^*_{ab}, and h_{ab} [15]. The subscripts indicate that the quantities are calculated from the rectangular coordinates a^* and b^*. L^* is the lightness of the color and corresponds to the vertical axis in the coordinate system. The chroma is C^*_{ab} corresponding to the distance to the center axis. The hue angle, h_{ab}, is the angle coordinate. The change in hue, ΔH^*_{ab}, is calculated from the change in hue angle Δh and the chroma values of the two colors in question. The method for calculating all color values can be found elsewhere [15]. For all calculations of color values a standard illuminant D65 and the CIE 1964 10° observer have been used. A color difference in, e.g., ΔC^*_{ab} of approximately 2.3 corresponds to a just noticeable difference; however, this varies across the color space which is not visually uniform [20]. The color change between the planar surface and the surfaces with different α values has been calculated for each of the three pigments. The right column of Fig. 4 shows the results and in Table 1 are the color changes for some specific values of α listed. For all three pigments the major component of the color change is an increase in the chroma value. This means that the position in the color space is moving away from the achromatic center axis and the color becomes more clear. All colors also show a slight decrease in lightness due to the lowering of the total

Table 1. Simulated Color Changes Compared to the Color of a Flat Surface for Four Specific Values of α[a]

Sample		$\alpha = 0$	$\alpha = 0.25$	$\alpha = 0.5$	$\alpha = 0.75$
Blue	ΔL^*	−4.5	−3.3	−2.2	−1.1
	ΔC^*_{ab}	7.2	5.3	3.4	1.7
	ΔH^*_{ab}	−1.1	−0.80	−0.50	−0.23
Green	ΔL^*	−3.9	−2.9	−1.9	−0.9
	ΔC^*_{ab}	19	13	8.1	3.8
	ΔH^*_{ab}	−0.65	−0.39	−0.21	−0.089
Red	ΔL^*	−5.2	−3.8	−2.5	−1.2
	ΔC^*_{ab}	18	12	7.4	3.5
	ΔH^*_{ab}	8.0	4.7	2.6	1.1

[a]The tabulated values are from the results of Fig. 4.

reflectance. For the red pigment a significant change in hue is also seen.

The reflectance spectra of ABS samples with ARS in the surfaces were experimentally measured and are compared to those of the samples with planar surfaces in Fig. 5. As for the theoretically calculated results the reflectance drops for wavelengths with initial low reflectance. The calculated color coordinates of the measured colors are listed in Table 2 and the color differences between the flat and textured surfaces are listed in Table 3. Again it is found that the chroma increases for all three colors, while the other color attributes change less. This was also the case for the simple theoretical model in Fig. 4. To make a more direct comparison between the experimentally determined color changes and the model, the α values at which the experimental data fit the model best have been determined for each color using least square fits. The fitted α values are listed in Table 3 and the fits are also indicated in Fig. 4 where the experimental color changes are plotted at the found α values. Since α only is related to the surface it should be ideally the same for all three colors. It is seen that determined α values are between 0.1 and 0.2, implying a reduction of the reflectance at the surface to a level of 10%–20% of the original value.

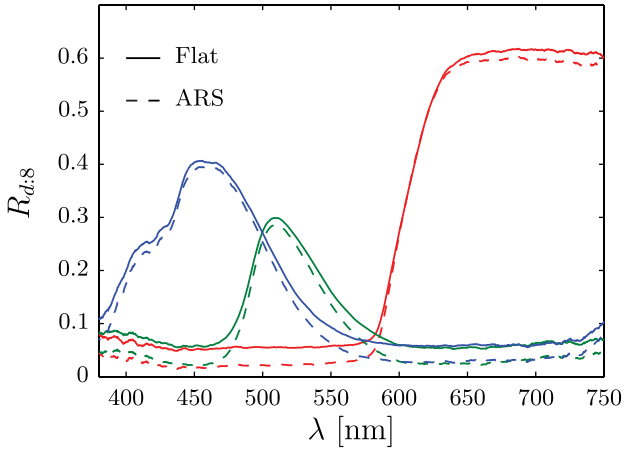

Fig. 5. Measured diffuse-direct reflectances for the three colors blue, green, and red for the case of planar surfaces (full lines) and surfaces with ARS (dashed lines). The corresponding color changes are given in Table 3.

Table 2. Color Coordinates Calculated from Experimentally Measured Reflectance Spectra (Fig. 5) for Samples with Flat Surfaces and with ARS

Sample	L^*	C^*_{ab}	h_{ab} [deg]
Blue flat	43.5	39.3	261
Blue w. ARS	39.3	44.7	259
Green flat	45.6	48.3	154
Green w. ARS	41.9	63.5	152
Red flat	42.2	51.9	29
Red w. ARS	37.8	67.1	36

Table 3. Experimentally Measured Changes in Cylindrical Color Coordinates, When Going from Flat Samples to Samples with ARS

Sample	ΔL^*	ΔC^*_{ab}	ΔH^*_{ab}	α_{fit}
Blue	−4.1	5.5	0.89	0.19
Green	−3.7	15	−1.5	0.15
Red	−4.4	15	7.2	0.10

This is somewhat lower than what is expected from previous investigations [14]. The discrepancy may be due to the simplifying assumptions of the model, such as the no scattering assumption and the assumption of α being independent on angle and wavelength.

The color changes described here are illustrated in Fig. 6, where samples of each of the three colors have been imprinted with a silicon master stamp, with ARS covering only half of the wafer. This leaves a polymer sample with the antireflective effect only being present on the right-hand side. The pictures are taken under diffuse lighting conditions.

In this paper, we have used diffuse light in the treatment of the surface. The change in color will not be the same if the samples were seen under strong point-like light sources. In this case it would depend on whether a specular reflection of one of the light sources is seen by the observer or not. In the case of a specular reflection being seen by the observer, the color difference between the flat and structured sample would be even more significant than observed with diffuse light. If no specular component was seen, there would be almost no color difference.

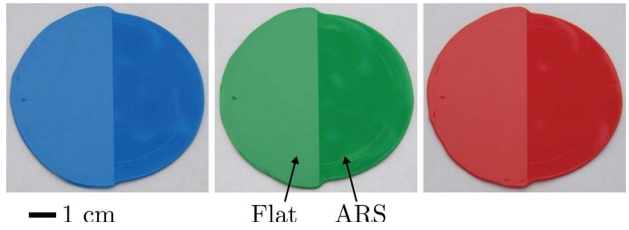

Fig. 6. Blue, green, and red ABS samples imprinted with a silicon stamp where half of the stamp was flat and the other half was covered with ARS. The left parts of the samples are flat and the right parts are with ARS.

5. Conclusion

It is found that by structural modification of the surface of a pigmented polymer it is possible to reduce the reflectance of the surface. This reduction in reflectance leads to a change in the reflected spectrum, which leads to a change in color appearance. For diffuse illumination it is found both theoretically and experimentally that the major part of the color change is an enhancement in chroma, which makes the color appear more clear and pure.

The authors acknowledge Claus H. Nielsen, DTU Danchip, for assistance with injection molding of substrates for embossing. The work was supported by the NanoPlast project funded by the Danish National Advanced Technology Foundation (File No. 007-2010-2).

References

1. C. G. Bernhard, "Structural and functional adaptation in a visual system," Endeavour **26**, 79–84 (1967).
2. P. B. Clapham and M. C. Hutley, "Reduction of lens reflexion by the moth eye principle," Nature **244**, 281–282 (1973).
3. S. Wilson and M. Hutley, "The optical properties of "moth eye" antireflection surfaces," Opt. Acta **29**, 993–1009 (1982).
4. H. Jung and K.-H. Jeong, "Monolithic polymer microlens arrays with antireflective nanostructures," Appl. Phys. Lett. **101**, 203102 (2012).
5. P. Lalanne and G. M. Morris, "Antireflection behavior of silicon subwavelength periodic structures for visible light," Nanotechnology **8**, 53–56 (1997).
6. Y. Kanamori, M. Sasaki, and K. Hane, "Broadband antireflection gratings fabricated upon silicon substrates," Opt. Lett. **24**, 1422–1424 (1999).
7. C.-H. Sun, P. Jiang, and B. Jiang, "Broadband moth-eye antireflection coatings on silicon," Appl. Phys. Lett. **92**, 061112 (2008).
8. C.-H. Sun, B. J. Ho, B. Jiang, and P. Jiang, "Biomimetic subwavelength antireflective gratings on GaAs," Opt. Lett. **33**, 2224–2226 (2008).
9. J. Tommila, V. Polojärvi, A. Aho, A. Tukiainen, J. Viheriälä, J. Salmi, A. Schramm, J. Kontio, A. Turtiainen, T. Niemi, and M. Guina, "Nanostructured broadband antireflection coatings on AlInP fabricated by nanoimprint lithography," Sol. Energy Mater. Sol. Cells **94**, 1845–1848 (2010).
10. C.-J. Yang, C.-L. Lin, C.-C. Wu, Y.-H. Yeh, C.-C. Cheng, Y.-H. Kuo, and T.-H. Chen, "High-contrast top-emitting organic light-emitting devices for active-matrix displays," Appl. Phys. Lett. **87**, 143507 (2005).
11. R. Singh, K. N. Narayanan Unni, A. Solanki, and Deepak, "Improving the contrast ratio of OLED displays: an analysis of various techniques," Opt. Mater. **34**, 716–723 (2012).
12. H.-R. Lee, D. Jae Kim, and K.-H. Lee, "Anti-reflective coating for the deep coloring of pet fabrics using an atmospheric pressure plasma technique," Surf. Coat. Technol. **142–144**, 468–473 (2001).
13. H. Becker and U. Heim, "Hot embossing as a method for the fabrication of polymer high aspect ratio structures," Sens. Actuators A **83**, 130–135 (2000).
14. A. B. Christiansen, J. Clausen, N. A. Mortensen, and A. Kristensen, "Minimizing scattering from antireflective surfaces replicated from low-aspect-ratio black silicon," Appl. Phys. Lett. **101**, 131902 (2012).
15. G. A. Klein, *Industrial Color Physics* (Springer, 2010).
16. M. Elias, P. Castiglione, and G. Elias, "Influence of interface roughness on surface and bulk scattering," J. Opt. Soc. Am. A **27**, 1265–1273 (2010).
17. S. Chandrasekhar, *Radiative Transfer* (Dover, 1960).
18. F. E. Nicodemus, J. C. Richmond, J. J. Hsia, I. W. Ginsberg, and T. Limperis, "Geometrical considerations and nomenclature for reflectance," Natl. Bur. Stand. (U.S.), Monogr. **160**, 1–52 (1977).
19. L. B. Wolff, "Diffuse-reflectance model for smooth dielectric surfaces," J. Opt. Soc. Am. A **11**, 2956–2968 (1994).
20. G. Sharma, *Digital Color Imaging Handbook* (CRC Press, 2002).